

SUPPLEMENTARY INFORMATION

How to Switch from a Poor PEDOT:X Oxygen Evolution Reaction (OER) to a Good One. A study on Dual Redox Reversible PEDOT/Metallacarborane.

Jewel Ann Maria Xavier^{†a}, Isabel Fuentes^{†a}, Miquel Nuez-Martínez^a, Zsolt Kelemen^a, Andreu Andrio^b, Clara Viñas^a, Vicente Compañ^c, and Francesc Teixidor^{a*}.

^a Institut de Ciència de Materials de Barcelona, ICMAB-CSIC, Campus Universitat Autònoma de Barcelona, 08193 Bellaterra, Barcelona, Spain.

^b Departamento de Física Aplicada, Universidad Jaume I, Avda. Sos Baynat s/n, 12071 Castellón de la Plana, Spain.

^c Escuela Técnica Superior de Ingenieros Industriales. Departamento de Termodinámica Aplicada, Universitat Politècnica de València, Camino de vera s/n, 46022- Valencia, Spain.

[†] These authors contributed equally.

*: Corresponding author: teixidor@icmab.es

INDEX:

Synthesis and characterization of Cs[1]-Cl₂

Figure S1. Cyclic voltammograms of a) Cs[1], b) Cs[1]-Cl₂, c)Cs[1]-Cl₄, d) Cs[1]-Cl₆ and e) Cs[1]-I₆ with ferroceneas internal reference in anhydrous acetonitrile.

Figure S2. High resolution XPS spectra of [1], PEDOT:[1] and PEDOT:[1]-Cl₆.

Figure S3. FTIR spectra of PEDOT:[1]-Cl_x (x=2,4 and 6), PEDOT:[1]-I₆ and PEDOT:PSS.

Figure S4. Thermogravimetric analysis of PEDOT:[1]-Cl_x (x=2,4 and 6), and PEDOT:PSS from 298-1173K.

Figure S5. Linear sweep voltammograms of a) PEDOT:[1]-Cl₂; b) PEDOT:[1]-Cl₄; c) PEDOT:[1]-Cl₆, inclusive of the deconvolution of the wave; d) PEDOT:[1]-I₆ and e) PEDOT:PSS in 0.1M Na₂SO₄ at 0.5mV/s.

Figure S6. Bode diagrams of a) PEDOT:[1]-Cl₂; b) PEDOT:[1]-Cl₄; c) PEDOT:[1]-Cl₆; d) PEDOT:[1]-I₆ and e) PEDOT:PSS at different temperatures from 20-160°C.

Figure S7. Temperature dependence of conductivity obtained from Bode diagram for a) PEDOT:[1]-Cl₂ (□); b) PEDOT:[1]-Cl₄ (□); c) PEDOT:[1]-Cl₆ (◆); d) PEDOT:[1]-I₆ (◆) and e) PEDOT:PSS (■).

Figure S8. Temperature dependence of the direct-current conductivity a) PEDOT:[1]-Cl₂ (□); b) PEDOT:[1]-Cl₄ (□); c) PEDOT:[1]-Cl₆ (◆); d) PEDOT:[1]-I₆ (◆) and e) PEDOT:PSS (■), for all the range of temperatures.

Figure S9. Linear sweep voltammetries of PEDOT:PSS (grey), PEDOT:[1], (blue) and PEDOT:[1]-Cl₆ (yellow) to compare their water oxidation catalytic power at a) pH=7 and b) pH=13.

Figure S10. OER confirmation in WOC in pH=7 with 1 mM of fluoresceine using GC-PEDOT:metallacarborane electrode to demonstrate the formation of O₂.

Figure S11: i vs v for PEDOT:Cs[*o*-COSAN] at pH=7 for both oxidative and reductive currents.

Table S1. Parameters of Gaussian function deconvoluted Co^{4+/3+} oxidation waves.

Synthesis and characterization of Cs[1]-Cl₂: To a solution of 1 equivalent of

Cs[**1**] (148.4 mg) and 2.3 equivalent of N-Chlorosuccinimide (100 mg) in 50 mL of tetrahydrofuran in a 100 mL round bottomed flask was heated for 24 hours at 58°C. Then, the volatiles were removed in the rotavapor and the product was extracted with diethyl ether (15 mL) and 1 M aqueous HCl three times (3 x 15 mL) to remove all the impurities. After the extraction, the organic layer was dried over MgSO₄, filtered and the liquid was evaporated and dissolved in the minimum volume of water. An aqueous solution containing an excess of CsCl was added, resulting in the formation of an orange precipitate. This Cs[**1**]-Cl₂ was filtered off, washed several times with water and dried.

Characterization of Cs[**1**]-Cl₂: ATR-FTIR (cm⁻¹): ν 3051 (w, C_c-H), 2606, 2537 (s, B-H). MALDI-TOF-MS: m/z calc for [**1**]-Cl₂⁻: 391; m/z found (%): 368 [**1**]-Cl₁, 1.60%, 392 [**1**]-Cl₂, 96.97% and 427 [**1**]-Cl₃, 1.43%. ¹H{¹¹B} NMR (300.13 MHz, CD₃OCD₃): δ = 4.31 (br s, 4H, C_c-H), 3.42, 3.19, 2.94, 2.77, 2.15, 1.76, 1.70 (br s, 14H, B-H). ¹¹B NMR (96.29 MHz, CD₃OCD₃): δ = 14.27, 1.74, 3.63, -17.23, -23.52.

Figure S1. Cyclic voltammograms of a) Cs[1], b) Cs[1]-Cl₂, c)Cs[1]-Cl₄, d) Cs[1]-Cl₆ and e) Cs[1]-I₆ with ferrocene as internal reference in anhydrous acetonitrile.

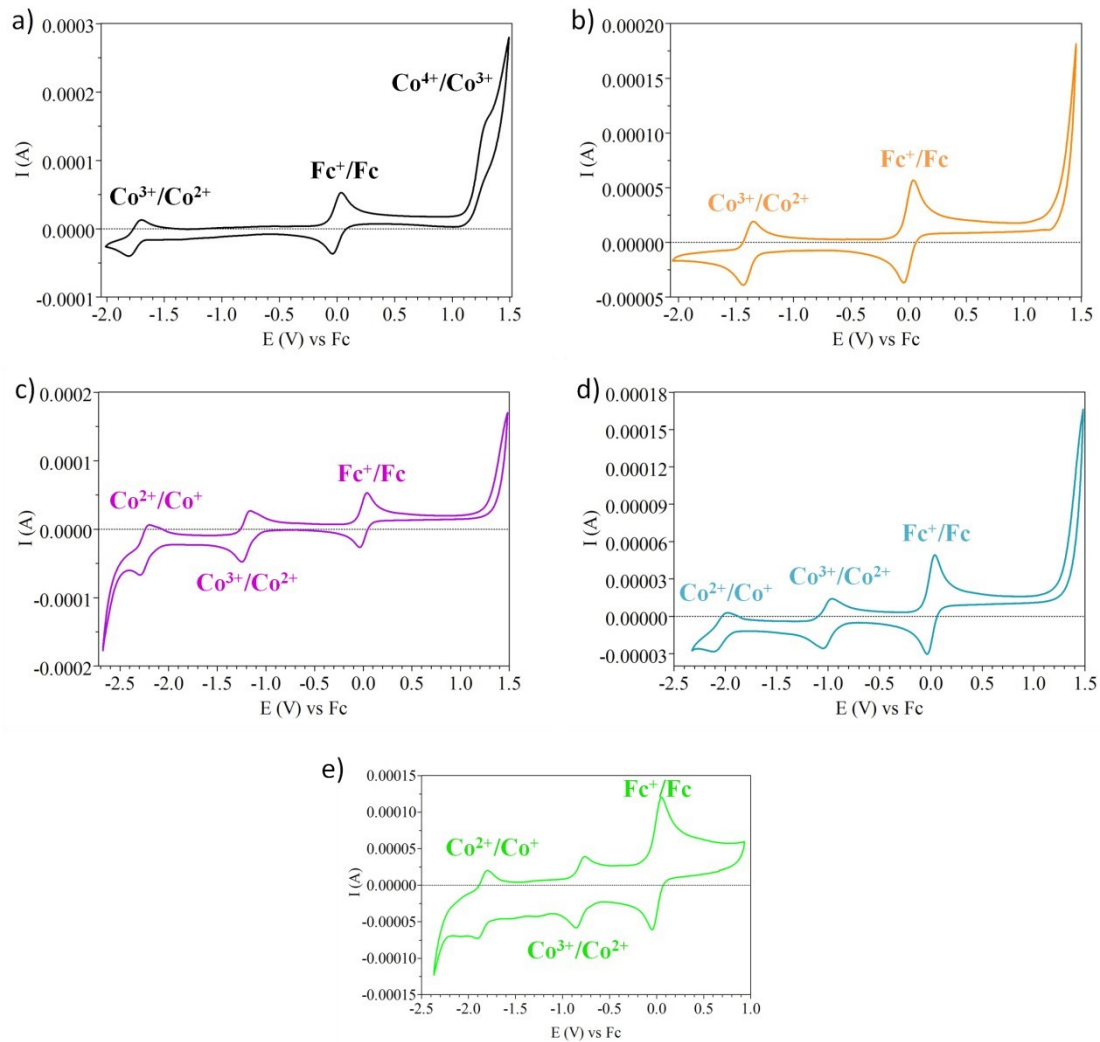


Figure S2. High resolution XPS spectra of [1], PEDOT:[1] and PEDOT:[1]-Cl₆.

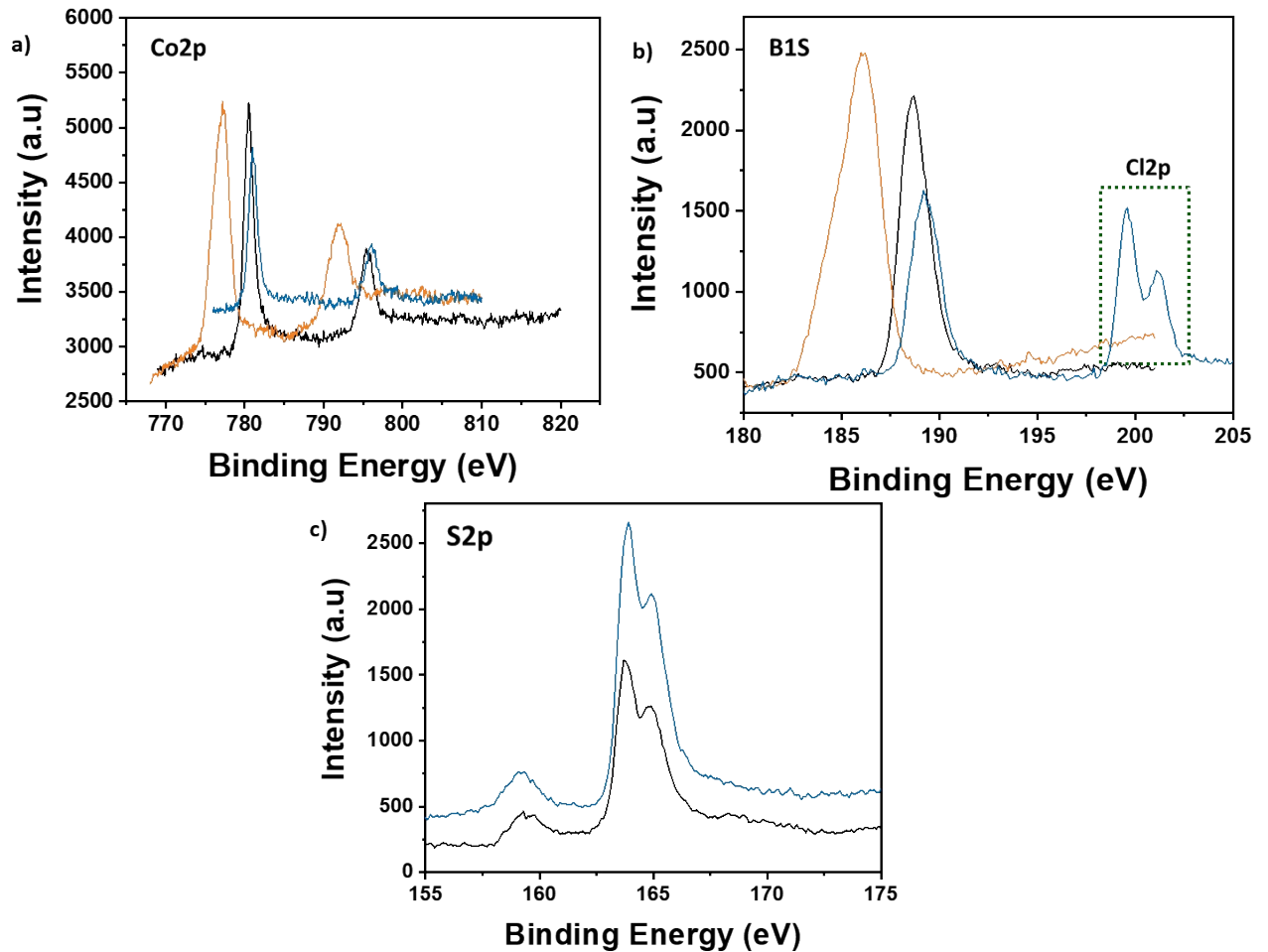


Figure S3. FTIR spectra of PEDOT:[1]-Cl_x (x=2,4 and 6), PEDOT:[1]-I₆ and PEDOT:PSS.

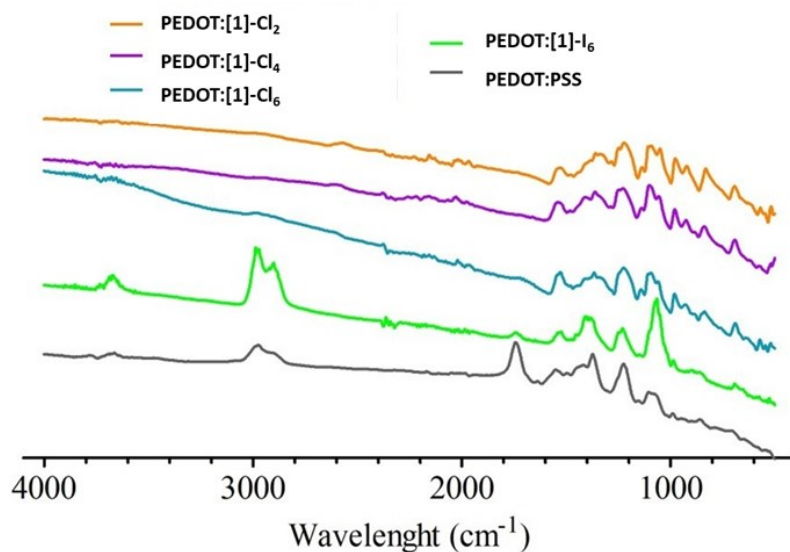


Figure S4. Thermogravimetric analysis of PEDOT:[1]-Cl_x (x=2,4 and 6), and PEDOT:PSS from 298-1173K.

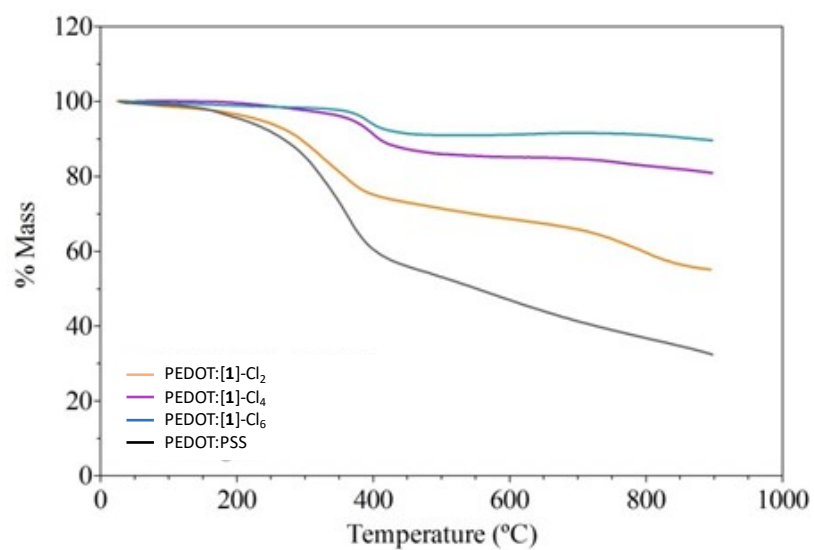


Figure S5. Linear sweep voltammograms of a) PEDOT:[1]-Cl₂; b) PEDOT:[1]-Cl₄; c) PEDOT:[1]-Cl₆, inclusive of the deconvolution of the wave; d) PEDOT:[1]-I₆ and e) PEDOT:PSS in 0.1M Na₂SO₄ at 0.5mV/s.

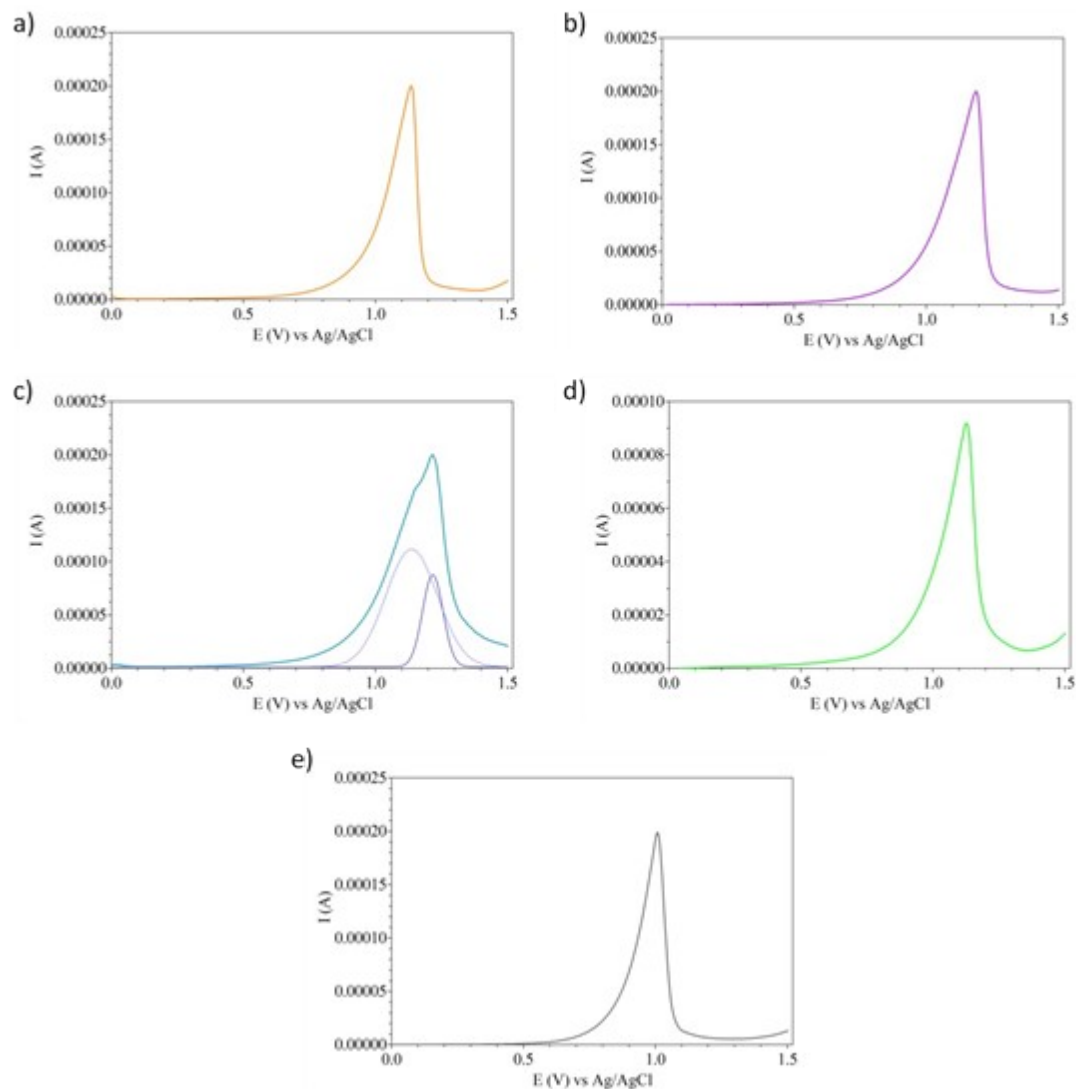


Figure S6. Bode diagrams of a) PEDOT:[1]-Cl₂; b) PEDOT:[1]-Cl₄; c) PEDOT:[1]-Cl₆; d) PEDOT:[1]-I₆ and e) PEDOT:PSS at different temperatures from 20-160°C.

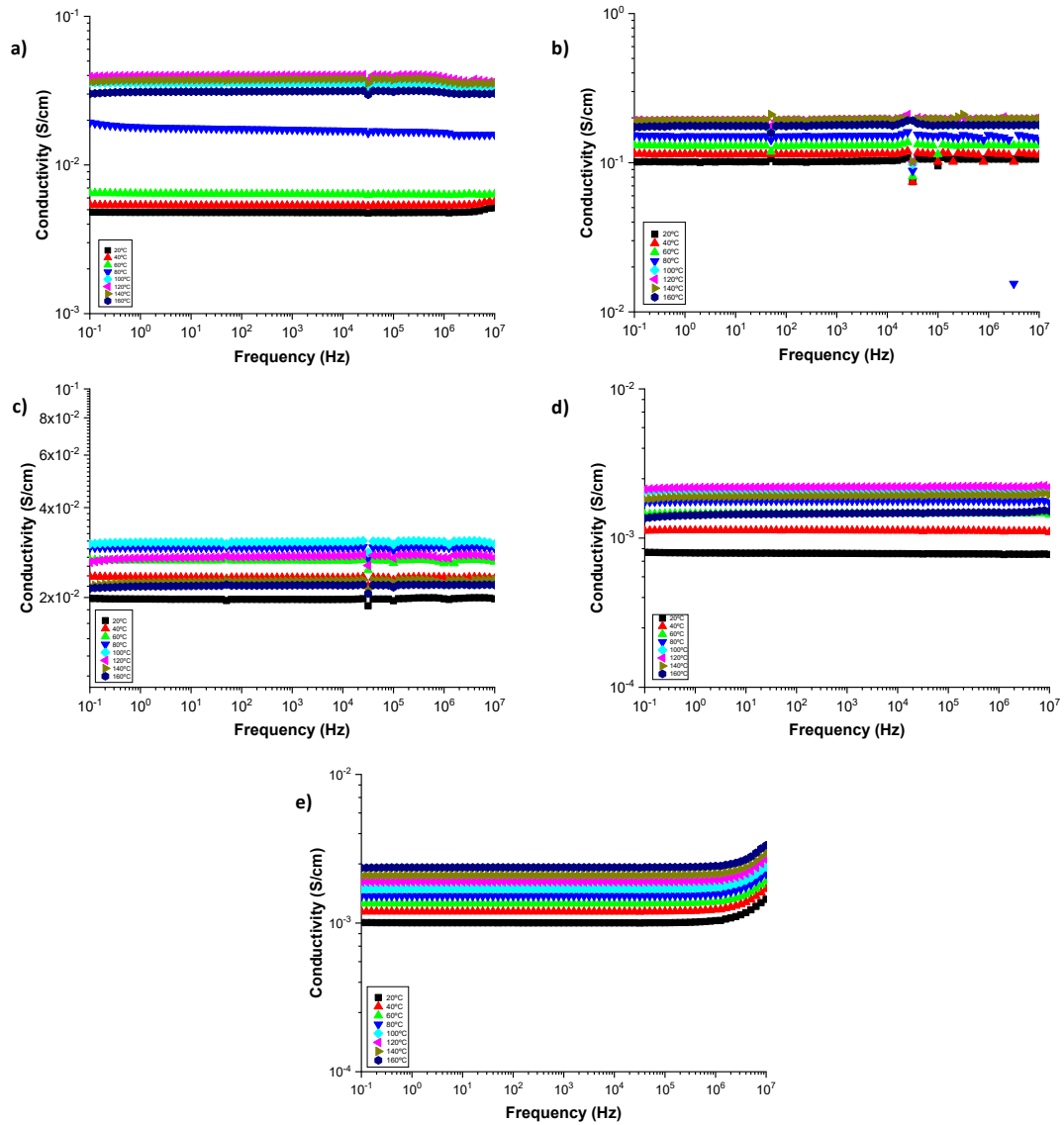


Figure S7. Temperature dependence of conductivity obtained from Bode diagram for a) PEDOT:[1]-Cl₂ (■); b) PEDOT:[1]-Cl₄ (□); c) PEDOT:[1]-Cl₆ (◆); d) PEDOT:[1]-I₆ (◆) and e) PEDOT:PSS (■).

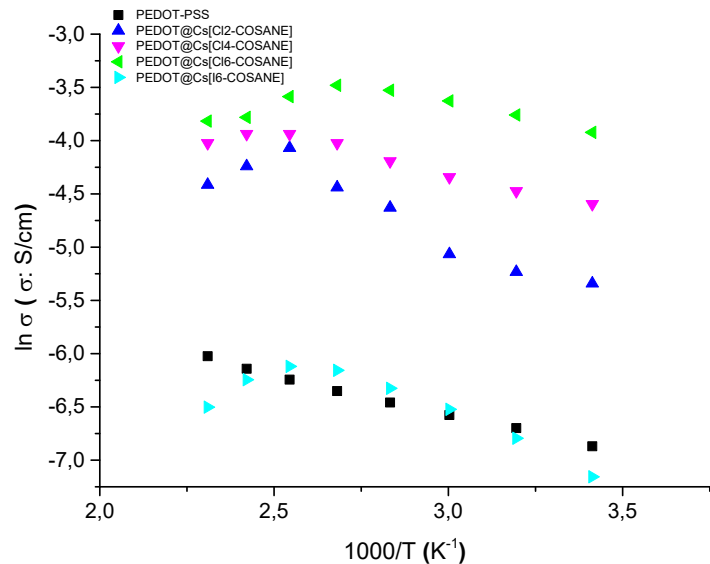


Figure S8. Temperature dependence of the direct-current conductivity a) PEDOT:[1]-Cl₂ (■); b) PEDOT:[1]-Cl₄ (□); c) PEDOT:[1]-Cl₆ (◆); d) PEDOT:[1]-I₆ (◇) and e) PEDOT:PSS (■), for all the range of temperatures.

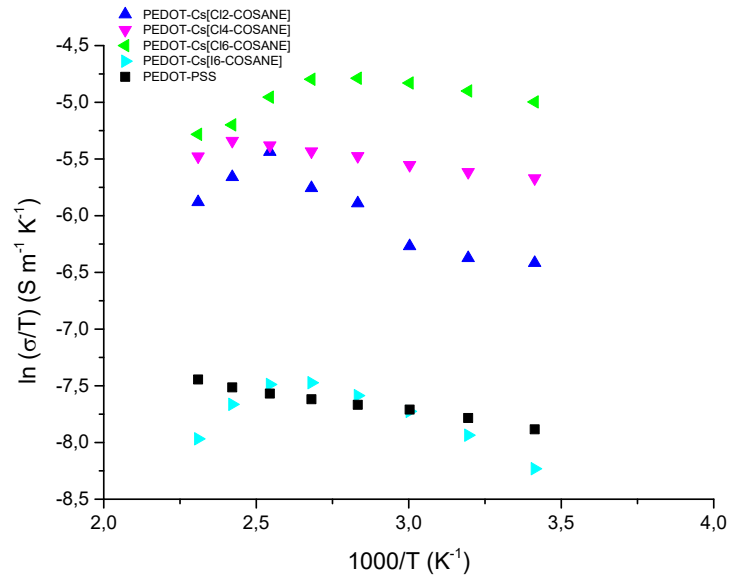


Figure S9. Linear sweep voltammetries of PEDOT:PSS (grey), PEDOT:[1], (blue) and PEDOT:[1]-Cl₆ (yellow) to compare their water oxidation catalytic power at a) pH=7 and b) pH=13.

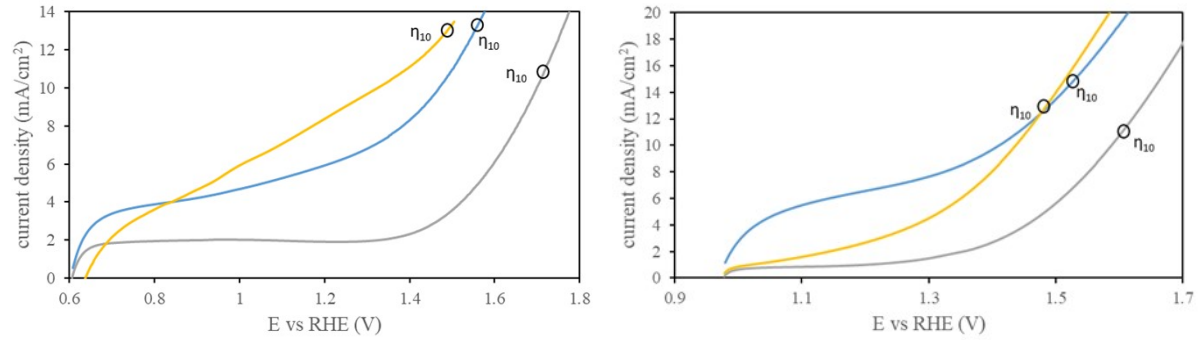


Figure S10. OER confirmation in WOC in pH=7 with 1 mM of fluorescein using GC-PEDOT:metallacarborane electrode to demonstrate the formation of O₂.

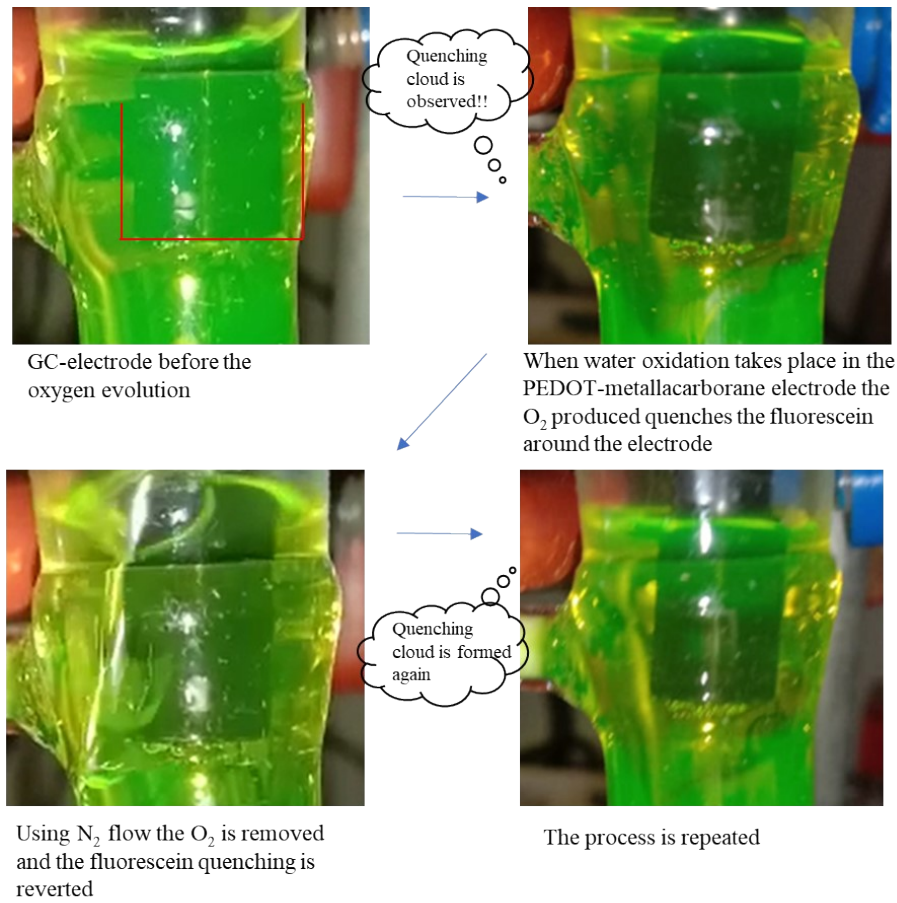


Figure S11: i vs v for PEDOT:Cs[*o*-COSAN] at pH=7 for both oxidative and reductive currents.

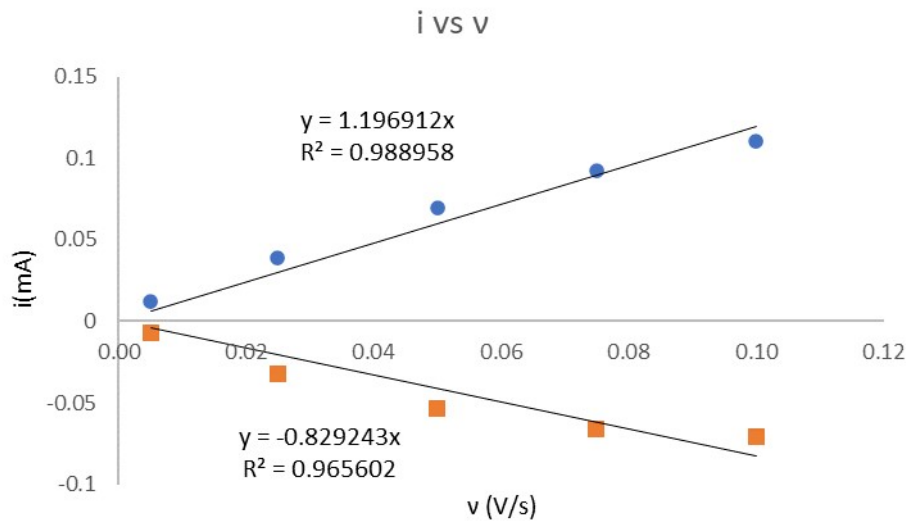


Table S1. Parameters of Gaussian function deconvoluted Co^{4+/3+} oxidation waves as the summatory of square error.

Sample	pH	Peak Value	Area	SD	Σ Error ²
PEDOT:[1]	7	1.2451	1.0626	0.1912	1.5366
PEDOT:[1]-Cl ₆	7	1.1867	2.139	0.182	22.269
PEDOT:[1]	13	1.2331	0.267	0.093	1.4822
PEDOT:[1]-Cl ₆	13	1.1731	0.1697	0.1020	1.3907